Neutral argon density profile determination by comparison of spectroscopic measurements and a collisional-radiative model (invited)

Amy M. Keesee[a] and Earl E. Scime
Department of Physics, West Virginia University, Morgantown, West Virginia 26506-6315

(Received 2 May 2006; presented on 10 May 2006; accepted 12 June 2006; published online 22 September 2006)

Neutral atoms play important roles in non-fully-ionized plasmas. In helicon sources, neutral pumping and neutral damping of waves are poorly understood. Measurement of the spatial distribution of neutral atoms is possible with spectroscopic diagnostics such as laser-induced fluorescence (LIF) and passive emission spectroscopy. However, these measurements typically apply to an excited neutral atom state, rather than the entire neutral population. With a collisional-radiative (CR) model employing Langmuir probe measured electron parameters in argon helicon source plasmas, we have reproduced LIF and emission spectroscopy measured radial profiles for three excited neutral states. The CR model indicates a neutral depletion on axis of at least 60%. Simple calculations based on measured edge neutral pressures and peak plasma densities significantly underestimate the degree of ionization in the core of the helicon plasma. © *2006 American Institute of Physics.* [DOI: 10.1063/1.2219440]

I. INTRODUCTION

The Ar I diode laser-based laser-induced fluorescence scheme used in this work was developed to investigate several important unanswered questions about the role played by neutral atoms in helicon source plasmas.[1] For example, measurements of Alfvén wave dispersion relations in helium helicon plasmas appear to be consistent with wave damping due to ion-neutral collisions.[2] However, the neutral densities required for consistency between the measured and theoretically predicted dispersion relations were much lower than expected given the measured neutral pressure at the edge of the source. Given the edge neutral pressure values, electrostatic probe and microwave interferometer plasma density measurements indicated that in the center of the discharge, the helium plasma was only 3% ionized. The wave measurements were consistent with a much higher ionization fraction near the center of the discharge. Other helicon source experiments also appear to be consistent with a hollow neutral radial density profile.[3] In fact, Boswell and Porteous postulated that fully ionized plasmas in the center of helicon discharges were required for pressure balance between the hot plasma in the center and the dense, cold neutrals at the plasma edge.[4] However, experimental confirmation of hollow neutral density profiles in helicon sources has been limited.[5]

The phenomenon of neutral pumping, whereby neutral atoms are ionized and then the ions are accelerated by the presheath electric field towards the chamber wall where they recombine and are pumped away, has also been investigated by several groups.[5–7] Such investigations found that helicon source plasma models best fit experimental measurements when neutral pumping, i.e., hollow neutral profiles, are included. In previous work on ion heating and ion flows in our helicon source experiment,[8–10] ion-neutral and electron-neutral collisions were identified as important mechanisms for wave damping, flow thermalization, and ion heating. In fact, edge-localized ion heating in cylindrically symmetric plasmas (observed in our experiments) is believed to be evidence of damping of the important edge-localized slow waves in the helicon source.[11–13] There is considerable debate about the possible existence of a population of energetic electrons in helicon sources.[14–16] Since such electrons would significantly affect excited neutral state populations, excited state neutral profiles that can only be explained by the presence of energetic electrons would be strong evidence for their existence.[17]

Laser-induced fluorescence (LIF) and passive emission spectroscopy can be used to measure the spatial distribution of temperatures, densities, and flow velocities of the neutral atoms. Since these measurements apply to an excited neutral atom state, rather than the entire neutral population, a collisional-radiative model (CR) is used to relate the densities of the excited states to the ground state if the electron density and energy distribution are known. With a CR model employing Langmuir probe measured electron parameters for argon helicon source plasmas, we have reproduced LIF and emission spectroscopy measured radial profiles for three excited neutral states.

II. EXPERIMENTAL APPARATUS

The hot helicon experiment (HELIX) vacuum chamber is a 61 cm long, Pyrex tube 10 cm in diameter connected to a 91 cm long, 15 cm diameter, stainless steel chamber (see Fig. 1). The chamber has one set of four 6 in. Conflat™ crossing ports in the center of the chamber and two sets of four 2 $\frac{3}{4}$ in. Conflat™ crossing ports on either side that are

[a]Electronic mail: ams_510@yahoo.com

 © 2006 American Institute of Physics

Downloaded 22 Sep 2006 to 157.182.109.55. Redistribution subject to AIP license or copyright, see http://rsi.aip.org/rsi/copyright.jsp

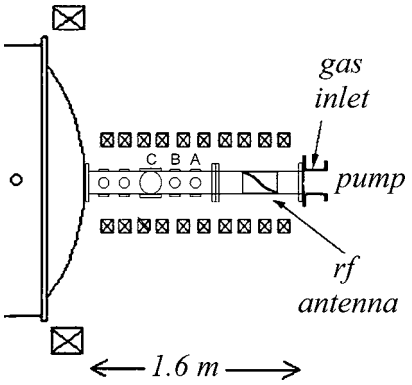

FIG. 1. Schematic of HELIX indicating location of (A) Baratron gauge, (B) Langmuir probe, and (C) LIF and spectroscopy collection optics.

used for LIF and spectroscopy diagnostic access. The stainless steel chamber opens into a 2 m diameter space chamber, the large experiment on instabilities and anisotropies (LEIA).[18] The opposite end of the Pyrex tube is attached to a glass tee. Ten electromagnets produce a steady state axial magnetic field of 0–1200 G in the source. An MKS mass flow controller located in the glass tee is used to introduce gas into the vacuum chamber. Neutral pressures are measured by a Balzers PKR250 full range pressure gauge located in the glass tee (operating pressures with discharge on) and by a Baratron pressure gauge located 35 cm downstream of the antenna (fill pressures without discharge). Plasmas are created at neutral pressures ranging from 0.1 to 100 mTorr. rf power of up to 2.0 kW over a frequency range of 6–18 MHz is coupled into a 19 cm half-wave, right-handed helix antenna to create the steady state plasma. Characteristic electron temperature and densities in HELIX are $T_e \approx 4$ eV and $n \approx 1 \times 10^{13}$ cm^3 as measured with a rf compensated Langmuir probe[19] located 50 cm downstream of the antenna.

The 1.5 MHz bandwidth Sacher Lasertechnik SAL-670-15 diode laser used for LIF was mounted in a Littrow external cavity and had a power output of $\leqslant$15 mW and a mode-hop-free tuning range of up to 10 GHz ($\approx$0.014 nm).[20] Wavelength scanning is accomplished by varying the voltage on a piezoelectric controlled grating located within the laser cavity. A National Instruments input/output (I/O) card provides the voltage ramp to scan the laser frequency and the linearly polarized laser is mounted on a vibration-isolated platform. The laser light is directed into the plasma with a series of mirrors and beam splitters mounted on the vacuum chamber and the laser table. The optical configuration is described in detail in Ref. 20. A tightly focused set of optics, mounted on a radially scanning assembly located at the crossing ports 65 cm downstream of the antenna, collects the fluorescence light perpendicular to the injected beam and sends the light through a fiber optic cable to a filtered (1 nm wide bandpass) Hamamatsu infrared detector. The detector signal is composed of fluorescence radiation, electron-impact induced radiation, and electronic noise. A mechanical chopper operating at a few kilohertz is used to modulate the laser beam before it enters the vacuum chamber and a Stanford Research Systems SR830 lock-in amplifier is used to eliminate all noncorrelated signals. Lock-in amplification is indispensable since the electron-impact induced emission is several orders of magnitude larger than the fluorescence signal. The laser wavelength is tuned to the appropriate transition and monitored for wavelength drift or hops during each scan with a Burleigh WA-1500 wavemeter.

A McPherson™ model 209 scanning monochromator, consisting of a 1.3 m Czerny-Turner system with a 120×140 mm^2 grating is used for the passive emission spectroscopy diagnostic. A computer-controlled stepper drive rotates the grating in order to select the desired detection wavelength. The detector is an air cooled Santa Barbara Instruments Group ST-7XEAI dual autofocusing charge coupled device (CCD) camera. Light emitted by the plasma is collected by a set of optics mounted on a vertically scanning assembly located at the crossing ports 65 cm downstream of the antenna, and is focused into a fiber optic cable attached to the entrance slit of the monochromator.

III. EXPERIMENTAL MEASUREMENTS

A. Laser-induced fluorescence

Complete details of the argon neutral LIF scheme used with our low power, tunable diode laser have been published previously.[1] Because the initial state of the Ar I LIF sequence is not a metastable state, the scheme requires an electron-impact, collisional excitation transfer to populate the initial state.

Figure 2 shows an energy level diagram of neutral argon. Our three level LIF scheme for Ar I uses laser emission at 667.9125 nm (in vacuum) to pump the $4s[3/2]_1$ state (state 3 in Fig. 2) to the $4p'[1/2]_0$ (state 11), which then decays to the $4s'[1/2]_1$ state (state 5) while emitting a photon at 750.5934 nm. This scheme is indicated in Fig. 2 by a solid arrow for the pump wavelength and a dashed arrow for the fluorescence wavelength. While the $4s[3/2]_1$ state is not a ground or metastable state, we expected a sufficient population for LIF due to direct excitation from the ground state and electron-impact excitation transfers from nearby metastable states $4s[3/2]_2$ and $4s'[1/2]_0$ (states 2 and 4, respectively) when operating at high ($>$10.5 mTorr) pressure.

To obtain reasonable Ar I LIF signal-to-noise ratio, the source was operated at pressures above 10.5 mTorr (operating pressure). Optimal signal-to-noise ratio was achieved for neutral pressures of approximately 17 mTorr (operating pressure). These relatively high neutral pressures provide the collision rates necessary to populate the initial $4s[3/2]_1$ state from the nearby metastable states.

The LIF signal is directly proportional to the density of the pump state in the collection volume:[21]

$$I \propto \frac{d\Omega}{4\pi} A_{11,5} \int d^3x \int d^3v N_3(x,v) \frac{B_{11,3}}{4\pi} \int_0^\infty d\nu \times L_{11,3}(\nu,v) W(x,\nu), \quad (1)$$

where $d\Omega$ is the detector's solid angle, $A_{11,5}$ is the Einstein transition coefficient from state 11 to 5, N_3 is the phase space density of state 3, $B_{11,3}$ is the Einstein absorption coefficient from 3 to 11, $L_{11,3}$ is the absorption line shape of the 3 to 11

Downloaded 22 Sep 2006 to 157.182.109.55. Redistribution subject to AIP license or copyright, see http://rsi.aip.org/rsi/copyright.jsp

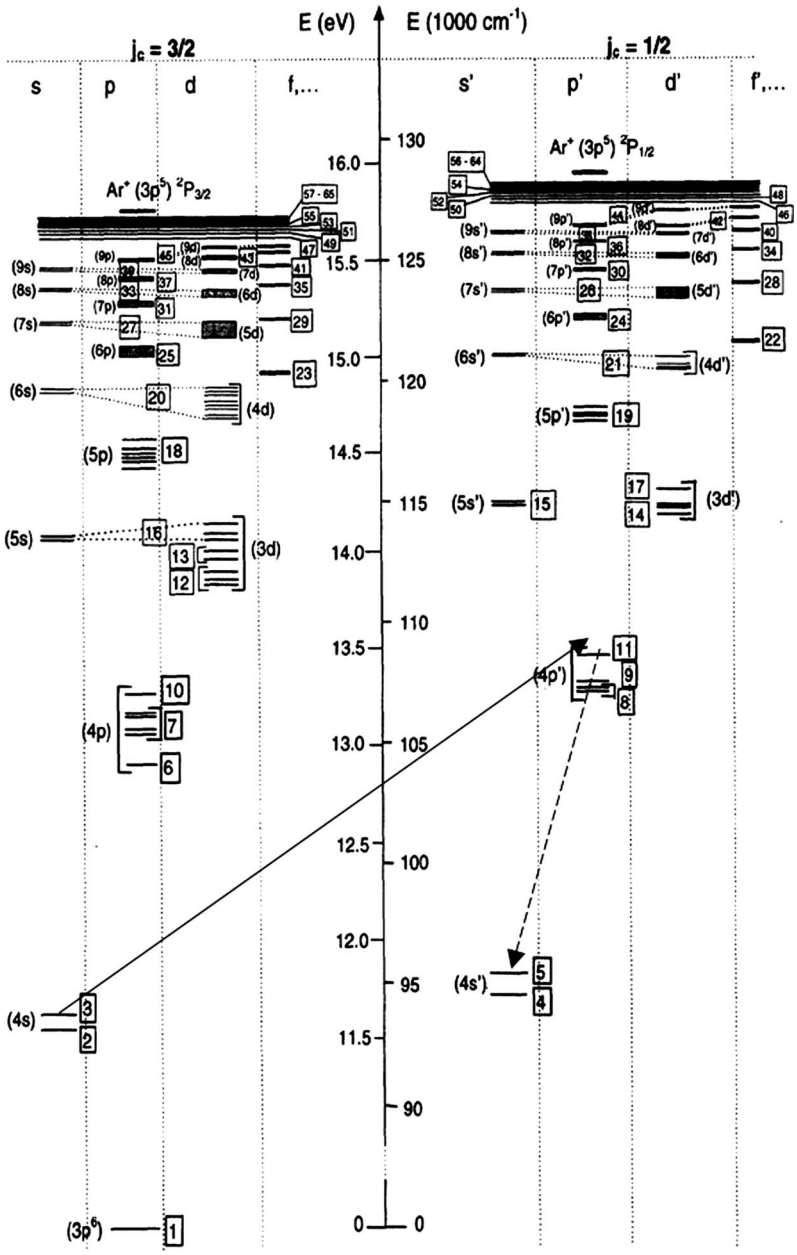

FIG. 2. Energy level diagram of argon with identifying numbers for each of the 65 effective levels used in the CR model. The LIF pump (solid) and fluorescence (dashed) lines are indicated.

transition, and W is the laser intensity line shape. The laser linewidth is on the order of a megahertz.[22] For typical helicon source argon plasma parameters, the total absorption line shape is a convolution of thermal (Doppler) broadening and Zeeman splitting. Because the Doppler width and Zeeman splittings are on the order of a gigahertz, other effects such as the natural linewidth of the line and Stark broadening are ignorable. For the specific Ar I transition used in this work, the Zeeman splitting yields three components.[23] For the π transition, the magnetic orbital quantum number for each level is the same ($\Delta M=0$). This transition is unshifted from the central wavelength and is linearly polarized along the magnetic field. For the two circularly polarized σ transitions, the magnetic orbital quantum number for each level is different ($\Delta M=\pm 1$). The line shifts for the $\pm\sigma$ transitions in a 1 kG magnetic field are $\Delta\lambda=\pm 2.08\times 10^{-2}$ Å.[24] Relative intensities of all three Zeeman components obey $I_\pi=2\ I_\sigma$.

When the polarization axis of the laser is oriented parallel to the axial magnetic field (perpendicular laser injection), only the π transition is pumped. Because only a single transition is pumped in the Ar I LIF measurements, Eq. (1) can be integrated over the essentially delta function laser line shape to yield a LIF intensity that is proportional to the bulk flow shifted Maxwellian distribution of state 3 neutral atoms:[25]

$$I(\nu)=I(\nu_0)\exp\left[\frac{-(\nu-\nu_0-V_o\nu_0/c)^2}{\alpha_D T_n}\right], \tag{2}$$

where $I(\nu)$ is the measured LIF signal, $I(\nu_o)$ is proportional to state 3 density, $(V_o\nu_0/c)$ is the overall Doppler shift of the distribution due to bulk flow of the neutrals, α_D scales the width of the thermal broadening for neutral argon of mass m_n ($\alpha_D=2k\nu_0/m_nc^2$), and T_n is the temperature of the neutrals in eV. Because the collection optics are focused along the injected laser beam, the measurement at each horizontal posi-

Downloaded 22 Sep 2006 to 157.182.109.55. Redistribution subject to AIP license or copyright, see http://rsi.aip.org/rsi/copyright.jsp

tion of the scanning assembly provides a radially and velocity resolved measurement of the state 3 neutral atom density. The relative state 3 neutral atom density as a function of radial position is obtained by integrating the LIF measurements over laser frequency. A two-dimensional (2D) optics scanning assembly is used to obtain profile measurements across the entire diameter of the plasma.[26]

B. Passive emission spectroscopy

The CCD count rate for a transition at a given wavelength λ is given by

$$I_p(\lambda) = I_\lambda T_\lambda \Psi_\lambda, \tag{3}$$

where T_λ is the transmission factor of the detection system and Ψ_λ is the sensitivity of the CCD. I_λ is the line intensity given by

$$I_\lambda = \frac{h\nu}{4\pi} A_{ki} n_k V \Omega, \tag{4}$$

where $h\nu$ is the energy of the transition ($\nu = c/\lambda$ is the frequency), A_{ki} is the Einstein transition probability for spontaneous emission, n_k is the number of atoms per cubic centimeter in level k, V is the detected plasma volume, and Ω is the solid angle subtended by the collection optics.[27] The relative density at each position is obtained by integrating over the measured emission line shape.

A matrix inversion method[28] is used to determine the radial density profiles from the line-integrated spectroscopic measurements at each vertical position of the collection optics. The inversion assumes cylindrical symmetry, yielding a profile across half the diameter of the plasma. The transitions measured by passive emission spectroscopy were state 11 (see Fig. 2) to state 3 at a wavelength of 667.9125 nm, state 11 to state 5 at 750.5934 nm, and the $4p[1/2]_0$ state (state 10 in Fig. 2) to state 3 at 751.6720 nm. Since this technique measures the density of the upper state for a transition, the 668 and 751 nm measurements should give the same radial profile when normalized.

IV. COLLISIONAL-RADIATIVE MODEL

The CR model used to determine the Ar I excited state populations for a given ground state density and electron distribution function was originally developed by Vlček,[29] then modified by Bogaerts *et al.*[30] into a one-dimentional (1D), spatially dependent model for a dc glow discharge. It describes the CR interaction between the 65 lowest energy levels of neutral argon shown in Fig. 2.[30] We modified the CR model to match the physical dimensions of HELIX and include only the CR processes relevant to our plasma conditions. The set of coupled equations describing the density $N(n,r)$ of each effective atomic level n at radial position r is given by

$$\frac{dN(n,r)}{dt} = R_{\text{gain}}(n,r) - R_{\text{loss}}(n,r) + D\frac{d^2N(n,r)}{dr^2}. \tag{5}$$

The processes described by R_{gain} and R_{loss} are as follows:

(1) Electron-impact excitation and deexcitation between all levels.
(2) Thermal argon atom impact excitation and deexcitation between all levels.
(3) Radiative decay between all levels.
(4) Electron-impact ionization from and three-body recombination to all levels.
(5) Thermal argon atom impact ionization from and three-body recombination to all levels.
(6) Radiative recombination to all levels.
(7) Two- and three-body collisions with thermal ground state atoms for metastable levels. (These collisions are negligible for the other levels because of their low densities.)
(8) Metastable-metastable collisions causing ionization of one of the atoms. (These collisions are negligible for the other levels because of their low densities.)

The third term on the right hand side of Eq. (5) includes the effects of diffusion for only the metastable states (the short lifetimes of the other excited state make their diffusion negligible). Additional details of the calculations used for each process are described by Vlček[29] and Bogaerts *et al.*[30]

The electron energy distribution functions (EEDFs) used in the code were based on rf-compensated Langmuir probe measured electron density and temperature radial profiles. As a first step, Maxwellian EEDFs were created based on the measured electron temperatures. An energetic electron beam could then be added to the Maxwellian distribution to study the effects of a beam on the neutral argon excited levels. The radial profiles of electron density, the EEDFs, and the fill pressure measured at the edge of the chamber are input variables for the code. The radial profile of the neutral ground state density in the code is varied to find the ground state profile that is most consistent with the spectroscopic and fluorescence measurements. The percentage of depletion at the center, P, and depletion width W are used to parametrize the neutral profile according to

$$\begin{aligned} &N(r) = N_0\left[m\left(\frac{2r}{W}\right)^2 - (1-P)\right], \quad -\frac{W}{2} \leqslant r \leqslant \frac{W}{2}, \\ &\quad m = P \text{ for } P < 0.5, \\ &\quad m = 1 - P \text{ for } P > 0.5, \\ &N(r) = N_0, \quad |r| > \frac{W}{2}, \end{aligned} \tag{6}$$

where N_0 is the neutral density found using the ideal gas law based on the input pressure and room temperature at the walls of the chamber. Because the Langmuir probe measurements were only obtained for half the diameter of the plasma, cylindrical symmetry is assumed in the CR model.

V. COMPARISON OF MODEL TO MEASUREMENTS

Each diagnostic measures the radial density profile of a specific excited atomic state. Thus, each of the measurements must be compared to the appropriate effective level in the CR model. The LIF measurements can be compared to state 3, the 668 and 751 nm emission lines can be compared to state 11, and the 752 nm emission line can be compared to

Downloaded 22 Sep 2006 to 157.182.109.55. Redistribution subject to AIP license or copyright, see http://rsi.aip.org/rsi/copyright.jsp

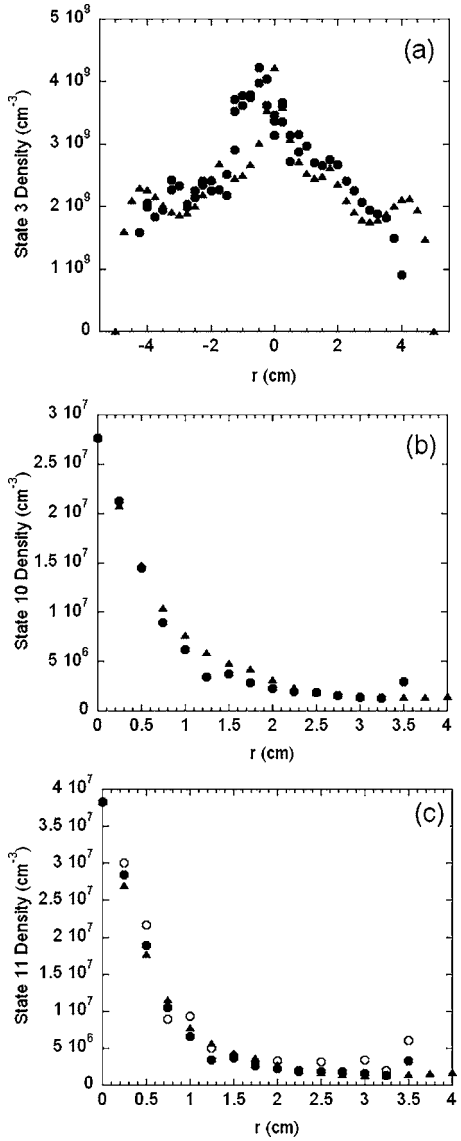

FIG. 3. Neutral argon excited state density vs radial position comparison between experimental data (circles) and CR model output (triangles) for a 3 cm wide depletion of 60%: (a) state 3, (b) state 10, and (c) state 11. In (c) the nearly identical measured profiles for the 667 nm (open circles) and 751 nm (filled circles) transitions are shown.

state 10 (see Fig. 2). Neither of the diagnostics is absolutely calibrated, so a peak-to-peak normalization is used for comparison of the measured radial density profile with the profile calculated by the CR model code.

Shown in Fig. 3 are comparisons of the measured LIF and emission profiles with CR model predictions for a helicon mode plasma operating at 300 W rf power, 750 G magnetic field, and 6.0 mTorr fill pressure/ 18.7 mTorr operating pressure. Note that the emission profiles are strongly peaked in the center of the discharge while the LIF profile is nearly flat. It is the requirement to generate strongly peaked emission profiles with a nearly flat LIF profile that places the strongest constraints on the neutral density profile. We found that the state 3 comparison, the LIF measurement–CR model comparison, was the most sensitive to CR model input changes. Most likely, this sensitivity results from state 3 being the lowest energy state examined and its being closer in

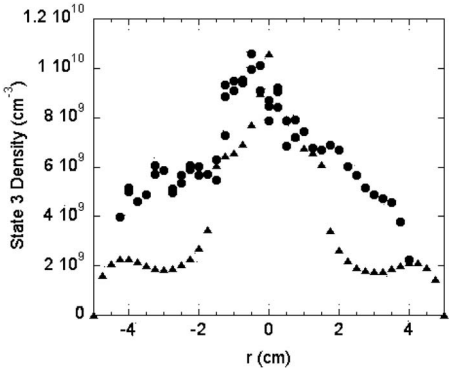

FIG. 4. Same as Fig. 3(a) for an 11% neutral depletion.

energy to the heavily populated metastable states than states 10 and 11. Thus, the radial structure in the measured plasma properties, e.g., electron temperature, is most evident in the CR model generated profiles for state 3. For the analysis presented here, matching the LIF data to state 3 in the CR model was the primary method of determining the best CR model inputs, while the spectroscopy data comparisons to states 10 and 11 provided additional confirmation of the model. The CR model input parameters of neutral density depletion and depletion width, and the presence and energy of an electron beam were varied, and the model output compared to the normalized data. After initial guesses were determined by hand, the best match was determined by a chi square test between the LIF data and CR model results. The asymmetry seen in the LIF measurement is a real phenomenon that we are unable to reproduce in the CR model and emission profiles due to the assumption of cylindrical symmetry in the CR model and the matrix inversion technique. However, over the region where both LIF measurements and Langmuir probe measurements were available, $r>0$, the model and measurements are in the best agreement.

The comparisons shown in Fig. 3 are for a 3 cm wide, 60% neutral density depletion in the center of the discharge ($P=0.6$, $W=3.0$). An energetic electron population, an electron beam, was not required to match the CR model results to the experimental measurements. A naive estimation of the depletion can be obtained from $N_{0\text{center}}=N_{0\text{edge}}-N_{i\text{center}}$, where quasineutrality is assumed so that $N_i=N_e$ and Langmuir probe measurements are used for N_e. This estimation yields an 11% depletion for these plasma parameters. For comparison, Fig. 4 shows the measured LIF profile with the CR model predictions for only an 11% depletion. The significantly more peaked LIF profile obtained with an 11% depletion is further evidence of the importance of neutral pumping, which depletes the neutral population to a greater extent than ionization alone. Comparison of Figs. 3(a) and 4 demonstrates that measurement of nearly uniform state 3 profile in a helicon source reflects a ground state neutral profile that is significantly depleted at the center. Having demonstrated that both combined LIF and emission spectroscopy measurements can provide nonperturbative measurements of the radial neutral density profile, the effects of col-

Downloaded 22 Sep 2006 to 157.182.109.55. Redistribution subject to AIP license or copyright, see http://rsi.aip.org/rsi/copyright.jsp

lisions with neutrals on wave damping, flow thermalization, momentum transport, and ion heating can now be examined quantitatively in helicon source plasmas.

ACKNOWLEDGMENTS

This work was performed with support from U.S. Department of Energy Grant No. DE-FG02-97ER54420 and NSF Grant No. PHY-0315356. The authors would like to thank R. E. Bell for calling their attention to the matrix inversion technique for radial profile reconstruction.

[1] A. M. Keesee, E. E. Scime, and R. F. Boivin, Rev. Sci. Instrum. **75**, 4091 (2004).
[2] C. Watts and J. Hanna, Phys. Plasmas **11**, 1358 (2004).
[3] G. R. Tynan, J. Appl. Phys. **86**, 5356 (1999).
[4] R. W. Boswell and K. Porteous, Appl. Phys. Lett. **50**, 1130 (1987).
[5] J. Gilland, R. Breun, and N. Hershkowitz, Plasma Sources Sci. Technol. **7**, 416 (1998).
[6] A. W. Degeling, T. E. Sheridan, and R. W. Boswell, Phys. Plasmas **6**, 1641 (1999).
[7] M. Yoon, S. C. Kim, H. J. Lee, and J. K. Lee, J. Korean Phys. Soc. **32**, L635 (1998).
[8] J. L. Kline, E. E. Scime, P. A. Keiter, M. M. Balkey, and R. F. Boivin, Phys. Plasmas **6**, 4767 (1999).
[9] E. E. Scime, P. A. Keiter, M. W. Zintl, M. M. Balkey, J. L. Kline, and M. E. Koepke, Plasma Sources Sci. Technol. **7**, 186 (1998).
[10] J. L. Kline *et al.*, Phys. Plasmas **10**, 2127 (2003).
[11] J. Kline, E. Scime, R. Boivin, A. M. Keesee, X. Sun, and V. Mikhailenko, Phys. Rev. Lett. **88**, 195002 (2002).
[12] J. L. Kline, E. Scime, R. Boivin, A. M. Keesee, and X. Sun, Plasma Sources Sci. Technol. **11**, 413 (2002).
[13] F. Anderegg, R. A. Stern, F. Skiff, B. A. Hammel, M. Q. Tran, P. J. Paris, and P. Kohler, Phys. Rev. Lett. **57**, 329 (1986).
[14] F. F. Chen, Plasma Phys. Controlled Fusion **33**, 339 (1991).
[15] F. F. Chen and D. D. Blackwell, Phys. Rev. Lett. **82**, 2677 (1999).
[16] A. W. Molvik, A. R. Ellingboe, and T. D. Rognlien, Phys. Rev. Lett. **79**, 233 (1997).
[17] C. Holland, J. H. Yu, A. James, D. Nishijima, M. Shimada, N. Taheri, and GJ. R. Tynan, Phys. Rev. Lett. **96**, 195002 (2006).
[18] E. E. Scime, P. A. Keiter, S. P. Gary, M. M. Balkey, R. F. Boivin, J. L. Kline, and M. Blackburn, Phys. Plasmas **7**, 2157 (2000).
[19] I. D. Sudit and F. F. Chen, Plasma Sources Sci. Technol. **3**, 162 (1994).
[20] R. F. Boivin and E. E. Scime, Rev. Sci. Instrum. **74**, 4352 (2003).
[21] M. J. Goeckner and J. Goree, J. Vac. Sci. Technol. A **7**, 977 (1989).
[22] Sacher Lasertechnik LLC, Instruction Manual, Hannah Arendt Str. 3–7, D35037 Marburg/Lahn, Germany (2000).
[23] L. Pauling and S. Goudsmit, *The Structure of Line Spectra* (McGraw-Hill, New York, 1930).
[24] G. Marr, *Plasma Spectroscopy* (Elsevier, New York, 1968).
[25] R. F. Boivin, West Virginia University Plasma Physics Laboratory Report No. PL-050, 2003 (unpublished). See EPAPS Document No. E-PHPAEN-10-003306 for "Zeeman splitting for LIF transitions and de-convolution techniques to extract ion temperatures" (June 2003). This document can be reached via a direct link in the online article's HTML reference section or via the EPAPS homepage (http://www.aip.org/pubservs/epaps.html).
[26] R. A. Hardin, X. Sun, and E. Scime, Rev. Sci. Instrum. **75**, 4103 (2004).
[27] W. Lochte-Holtgreven, *Plasma Diagnostics* (American Institute of Physics, New York, 1995).
[28] R. E. Bell, Rev. Sci. Instrum. **66**, 558 (1995).
[29] J. Vlček, J. Phys. D **22**, 623 (1989).
[30] A. Bogaerts, R. Gijbels, and J. Vlcek, J. Appl. Phys. **84**, 121 (1998).

Downloaded 22 Sep 2006 to 157.182.109.55. Redistribution subject to AIP license or copyright, see http://rsi.aip.org/rsi/copyright.jsp